The AAPS Journal, Vol. 18, No. 3, May 2016 (© 2016)
DOI: 10.1208/s12248-016-9886-1

Research Article

Pharmacodynamic Model of Hepcidin Regulation of Iron Homeostasis in Cynomolgus Monkeys

Wojciech Krzyzanski,[1,8] Jim J. Xiao,[2,3] Barbra Sasu,[4,5] Beth Hinkle,[6] and Juan Jose Perez-Ruixo[2,7]

Received 3 September 2015; accepted 9 February 2016; published online 25 February 2016

Abstract. Hepcidin (H_{25}) is a hormone peptide synthesized by the liver that binds to ferroportin and blocks iron export. In this study, H_{25} was inhibited by administration of single and multiple doses of an anti-H_{25} monoclonal antibody Ab 12B9m in cynomolgus monkeys. The objective of this analysis was to develop a pharmacodynamic model describing the role of H_{25} in regulating iron homeostasis and the impact of hepcidin inhibition by Ab 12B9m. Total serum H_{25} and Ab 12B9m were determined in each animal. Corresponding measurements of serum iron and hemoglobin (Hb) were obtained. The PD model consisted of iron pools in serum (Fe_S), reticuloendothelial macrophages (Fe_M), hemoglobin (Fe_{Hb}), and liver (Fe_L). The iron was assumed to be transported between the Fe_S, Fe_{Hb}, and Fe_M unidirectionally at rates k_S, k_{Hb}, and k_M. H_{25} serum concentrations were described by the previously developed PK model with the parameters fixed at their estimates. The serum iron and Hb data were fitted simultaneously. The corresponding estimates of the rate constants were $k_S/Fe_0 = 0.113$ h^{-1}, $k_M = 0.00191$ h^{-1}, and $k_{Hb} = 0.00817$ h^{-1}. The model-based IC_{50} value for the H_{25} inhibitory effect on ferroportin activity was 0.398 nM. The PD model predicted a negligible effect of Ab 12B9m on Hb levels for the tested doses. The presented PD model adequately described the serum iron time courses following single and multiple doses of Ab 12B9m. Ab 12B9m-induced inhibition of H_{25} resulted in a temporal increase in serum and liver iron and a decrease in the iron stored in reticuloendothelial macrophages.

KEY WORDS: ferrokinetics; hepcidin; iron kinetics; iron-restricted erythropoiesis.

INTRODUCTION

Iron is an essential trace metal incorporated into proteins responsible for cellular respiration, survival, and growth. However, the biggest iron requirement is for the generation of hemoglobin in red blood cells. Excess iron leads to the production of radicals, which damage cell membranes, proteins, and DNA, leading to cell death. Therefore iron uptake, excretion, and distribution are tightly regulated. Iron is available only through diet, and its distribution and retention in the body are controlled by sequestration and recycling mechanisms. Under normal conditions, only small amounts of iron are lost daily due to mucosal and skin epithelial cell sloughing. Given a moderate dietary iron uptake, iron distributed throughout tissues forms a (semi)closed system. Duodenal enterocytes absorb dietary iron and export the iron into the circulation. Iron circulates in plasma bound to transferrin. Most of the iron in the body is incorporated into hemoglobin in erythroid precursors and mature red blood cells. Reticuloendothelial macrophages recycle iron from senescent erythrocytes. Intracellular iron is also stored with ferritin in the liver, where it accounts for a third of the total iron. Approximately 10% of iron is present in muscle fibers (in myoglobin) and other tissues (1).

Hepcidin is a hormone peptide synthesized by the liver that binds to ferroportin in cell membranes, causes ferroportin internalization, and degradation, and thereby blocks iron export (2). Hepcidin is a key regulator responsible for systemic iron homeostasis, which has been suggested to be a strategic target for iron regulation in the treatment of various iron disorders, such as hyporesponsiveness to erythropoietin (3). During normal iron homeostasis, increased circulating iron levels upregulate hepcidin expression in the liver. High serum hepcidin levels decrease intestinal iron absorption and block iron export from tissue stores into the bloodstream in order to protect the body against excess total body iron accumulation. Conversely, low levels of circulating iron results in downregulation of hepcidin synthesis, allowing

Electronic supplementary material The online version of this article (doi:10.1208/s12248-016-9886-1) contains supplementary material, which is available to authorized users.

[1] Department of Pharmaceutical Sciences, University at Buffalo, Buffalo, New York, USA.
[2] Pharmacokinetics and Drug Metabolism, Amgen Inc, Thousand Oaks, California, USA.
[3] *Present Address:* Clinical Pharmacology, Clovis Oncology, San Francisco, California, USA.
[4] Oncology, Amgen Inc, Thousand Oaks, California, USA.
[5] *Present Address:* Research Oncology, Pfizer, San Francisco, California, USA.
[6] Comparative Biology and Safety Sciences, Amgen Inc, Thousand Oaks, California, USA.
[7] *Present Address:* Janssen Research and Development, Beerse, Belgium.
[8] To whom correspondence should be addressed. (e-mail: wk@buffalo.edu;)

an influx of bioavailable iron from the duodenal enterocytes and iron stores in tissues (4).

Ab 12B9m is a fully human immunoglobulin G subtype 2 monoclonal antibody that binds to cynomolgus monkey and human hepcidin (5). Administration of varying doses of Ab 12B9m in cynomolgus monkeys was able to suppress hepcidin, resulting in a temporary increase of serum iron levels (6). Such a perturbation of the hepcidin-iron regulation was used to estimate the hepcidin production and elimination rates, and also to provide unique iron kinetic data traditionally obtained by injecting tracer amounts of radioactive iron. These data are the subject of analysis presented in this report.

Iron kinetics in animals and humans has been studied for over 70 years with the seminal work of McCance and Widdowson (7) as one of the earliest. The primary experimental technique involves injection of tracer amounts of radioactive iron and measuring the signal over time in various tissues, including plasma, liver, spleen, bone marrow, and erythrocytes. Human data have been limited to blood measurements. Such kinetic data have been described by mathematical models with the tissue iron represented by compartments and iron uptake, elimination, and tissue distribution by means of first-order or more complex processes. The complexity of these models varied from few compartments (8,9) to many (10,11). The kinetic parameters have been estimated by fitting the available data by the model and used to establish tissue and animal-specific values for iron half-life or residence time, baseline concentration or amount, absorption and distribution rates, and others. Such values were compared with analogous parameters obtained experimentally by non-compartmental techniques (12–14). Ferrokinetics have been studied in normal and disease model animals, iron deficient and saturated, and under homeostatic or non-stationary conditions. Consequently, iron kinetics is relatively well understood. Mathematical models of iron data measured by biochemical methods such as plasma transferrin and ferritin are virtually nonexistent, largely due to the absence of external factors capable of perturbing iron homeostasis.

The objective of this study was to develop a pharmacodynamic model describing the role of hepcidin H_{25} in regulating iron homeostasis and investigate the impact of hepcidin inhibition by an anti-hepcidin monoclonal antibody Ab 12B9. The model was fitted to the serum iron data obtained after single and multiple doses of Ab 12B9m and resulted in estimates of ferrokinetic parameters as well as parameters characterizing the hepcidin inhibitory effect on ferroportin. These parameters were further used to simulate time courses of iron levels in the compartments that were not measured, which included hepatocytes and reticuloendothelial macrophages. Based on the simulated data, we were able to predict the consequences of neutralizing hepcidin on the iron-restricted erythropoiesis in patients with anemia treated with erythropoiesis-stimulating agents.

METHODS

Study Design

Data available from two studies conducted by Amgen Inc. in cynomolgus monkeys were used in this analysis. Cynomolgus monkeys (*Macaca fascicularis*), 2 to 5 kg in weight, were cared for in accordance to the Guide for the Care and Use of Laboratory Animals, 8th Edition (15). Animals were socially housed at an indoor, AAALAC, Intl-accredited facility in species-specific housing. All research protocols were approved by the Institutional Animal Care and Use Committee. Animals were fed a certified pelleted primate diet daily in amounts appropriate for the age and size of the animals and had *ad libitum* access to water via automatic watering system/water bottle. Animals were maintained on a 12:12-h light/dark cycle in rooms maintained at 18°C to 29°C and 30% to 70% humidity, and animals had access to enrichment opportunities. In the first study, male animals ($n = 18$) received a single dose of Ab 12B9m at 0.5, 5, or 50 mg/kg either by intravenous (IV) or subcutaneous (SC) administrations. In the second study, male and female cynomolgus monkeys ($n = 25$) received placebo, once weekly (q.w.) IV doses at 5, 40, and 300 mg/kg and once weekly SC doses of Ab 12B9m at 300 mg/kg for 4 weeks (5,6). For each group, three monkeys/sex/group were necropsied after 28 days of treatment, and then two monkeys/sex/group were necropsied after a 19-week recovery period. Pharmacokinetic data were collected from all animals up to study day 29 with intensive pharmacokinetic sampling after the first and fourth doses (study days 1 and 22). Total serum hepcidin and Ab 12B9m concentrations were determined in each animal. Corresponding measurements of serum iron were obtained. For the single-dose group, the sampling times were pre-dose, 0.5 and 4 h and 1, 2, 4, 7, 14, 21, 28, 42, 56, and 70 days after the injection. For the multiple-dose group, the blood samples for serum iron assessment were drawn at pre-dose, 0.5 and 4 h, 1, 2, 4, 7, and 21 days, 21 days and 0.5 h, 21 days and 4 h, and 22, 23, 24, 25, 28, 43, 57, 71, 85, 99, 113, 127, 141, and 154 days after the first injection. Additionally, hemoglobin levels were followed pre-dose and on days 28, 71, 113, and 154 following the first dose.

PD Model of Hepcidin Effect on Serum Iron

The total serum hepcidin and Ab 12 B9m serum concentrations were described by a PK model published elsewhere (6). The PK model equations and parameter values are presented in the Appendix. The free hepcidin serum concentration C_{H25} predicted by this model is used as a driving force for the effect on serum iron and hemoglobin concentrations described by a PD model. The input to the serum iron pool (Fe_S) is mostly due to sequestration of iron from the reticuloendothelial macrophages (Fe_M) and liver (Fe_L) iron pools. The amount of dietary iron absorbed from the gastrointestinal track in an adult human is about 2 mg/day (1), which is negligible compared with the above input from macrophage and liver, and consequently was not included in the model. The loss of serum iron is caused by incorporation of the iron into the hemoglobin produced by erythropoietic precursor cells in the bone marrow and storage of iron in the liver. The loss rate of iron utilized by muscle myoglobin and due to sloughing mucosal cells, desquamation, menstruation, or other blood loss was considered small and was not accounted for by the model. These assumptions reduced the PD model to four pools Fe_S, Fe_M, Fe_L, and Fe_{Hb}, where the latter denotes the amount of iron bound in the hemoglobin. A

schematic diagram of the model is shown in Fig. 1. The free hepcidin serum concentration C_{H25} inhibits the first-order transport rates k_M and k_{LS} of iron from the macrophages and liver pools, respectively. The loss rate of serum iron due to distribution to liver and hemoglobin pools was modeled as a first-order process, characterized by k_{SL}, and zero-order process, determine by k_S, respectively:

$$\frac{d\mathrm{Fe_S}}{dt} = k_M \frac{I(C_{H25})}{I(C_{H25,\,0})}\mathrm{Fe_M} + k_{LS}\frac{I(C_{H25})}{I(C_{H25,\,0})}\mathrm{Fe_L} - k_{SL}\mathrm{Fe_S} - k_S \quad (1)$$

where $I(C_{H25})$ denotes the inhibitory Hill sigmoidal function:

$$I(C_{H25}) = 1 - \frac{I_{max}{C_{H25}}^{\gamma}}{{IC_{50}}^{\gamma} + {C_{H25}}^{\gamma}} \quad (2)$$

and $C_{H25,\,0}$ is the baseline hepcidin serum concentration. The ratios in Eq. 1 were introduced so the inhibitory factor at the baseline condition would equal 1. The I_{max} denotes the maximum inhibition, IC_{50} is the hepcidin serum concentration eliciting 50% of the maximum inhibition and γ represents Hill sigmoidal shape factor. To reduce the number of model parameters the maximum inhibition was assumed to be 100% and, therefore, $I_{max} = 1$. We assumed that iron bound in hemoglobin, $\mathrm{Fe_{Hb}}$, is sequestered by macrophages of the reticuloendothelial system after red blood cell senescence:

$$\frac{d\mathrm{Fe_{Hb}}}{dt} = k_S - k_{Hb}\mathrm{Fe_{Hb}} - \mathrm{sam}\delta(t-t_1) - \mathrm{sam}\delta(t-t_2) \quad (3)$$

where $\mathrm{sam}\delta(t-t_i)$ represents a bolus loss of iron due to blood drawing at time t_i ($t_1 = 0$ and $t_2 = 21$ days). The macrophages release iron to the circulation at a first-order rate constant, k_M. This process is also inhibited by hepcidin, and it was described by the same inhibitory function as for the release of iron liver:

$$\frac{d\mathrm{Fe_M}}{dt} = k_{Hb}\mathrm{Fe_{Hb}} - k_M\frac{I(C_{H25})}{I(C_{H25,\,0})}\mathrm{Fe_M} \quad (4)$$

and

$$\frac{d\mathrm{Fe_L}}{dt} = k_{SL}\mathrm{Fe_S} - k_{LS}\frac{I(C_{H25})}{I(C_{H25,\,0})}\mathrm{Fe_L} \quad (5)$$

We assumed that all iron pools prior to treatment with Ab 12B9m remained at the baseline levels $\mathrm{Fe_{S0}}$, $\mathrm{Fe_{Hb0}}$, $\mathrm{F_{M0}}$, and $\mathrm{F_{L0}}$ determined by the system steady state:

$$\mathrm{Fe_{Hb0}} = \frac{k_S}{k_{Hb}} \quad (6a)$$

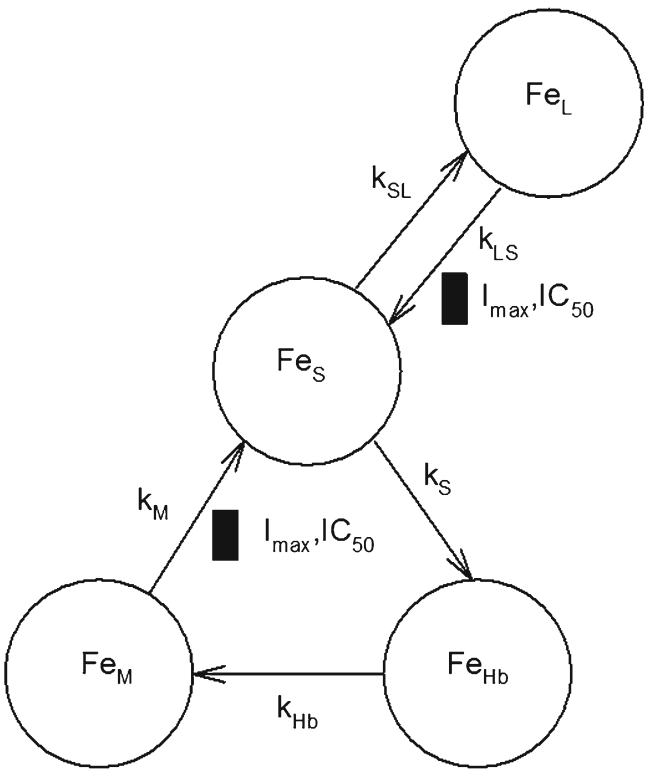

Fig. 1. Schematic diagram of the PD model of hepcidin effect on iron distribution. The model encompasses iron amounts in serum (Fe_S), hemoglobin (Fe_{Hb}), reticuloendothelial macrophages (Fe_M), and liver (Fe_L). Hepcidin inhibits the distribution of iron from the reticuloendothelial macrophages and liver pools (*black boxes*). I_{max} and IC_{50} are model parameters describing the hepcidin effect

$$\mathrm{Fe}_{M0} = \frac{k_S}{k_M} \tag{6b}$$

$$\mathrm{Fe}_{L0} = \frac{k_{SL}}{k_{LS}}\mathrm{Fe}_{S0} \tag{6c}$$

The baseline values were used as initial conditions for Eqs. 1 and 3–5. Since these values were not measured, the normalized variables were used:

$$\frac{d(\mathrm{Fe}_S/\mathrm{Fe}_{S0})}{dt} = \frac{k_S}{\mathrm{Fe}_{S0}}\frac{I(C_{H25})}{I(C_{H25,\,0})}\frac{\mathrm{Fe}_M}{\mathrm{Fe}_{M0}} + k_{SL}\frac{I(C_{H25})}{I(C_{H25,\,0})}\frac{\mathrm{Fe}_L}{\mathrm{Fe}_{L0}} - k_{SL}\frac{\mathrm{Fe}_S}{\mathrm{Fe}_{S0}} - \frac{k_S}{\mathrm{Fe}_{S0}} \tag{7}$$

$$\frac{d(\mathrm{Fe}_{Hb}/\mathrm{Fe}_{Hb0})}{dt} = k_{Hb} - k_{Hb}\frac{\mathrm{Fe}_{Hb}}{\mathrm{Fe}_{Hb0}} - \mathrm{Fr}\delta(t-t_1) - \mathrm{Fr}\delta(t-t_2) \tag{8}$$

$$\frac{d(\mathrm{Fe}_M/\mathrm{Fe}_{M0})}{dt} = k_M\frac{\mathrm{Fe}_{Hb}}{\mathrm{Fe}_{Hb0}} - k_M\frac{I(C_{H25})}{I(C_{H25,0})}\frac{\mathrm{Fe}_M}{\mathrm{Fe}_{M0}} \tag{9}$$

$$\frac{d(\mathrm{Fe}_L/\mathrm{Fe}_{L0})}{dt} = k_{LS}\frac{\mathrm{Fe}_S}{\mathrm{Fe}_{S0}} - k_{LS}\frac{I(C_{H25})}{I(C_{H25,0})}\frac{\mathrm{Fe}_L}{\mathrm{Fe}_{L0}} \tag{10}$$

where $\mathrm{Fr} = \mathrm{sam}/\mathrm{Fe}_{Hb0}$ denotes the fraction of the baseline iron hemoglobin lost due to blood drawing. The baseline relationship Eqs. 6a, 6b, and 6c were used to substitute terms from Eqs. 1 and 3–5.

Data Analysis

The naïve pooled serum iron data (without between subject variability) for each route of administration and dose were simultaneously fitted according to the following equation:

$$C_{Fe} = C_{Fe0}\frac{\mathrm{Fe}_S}{\mathrm{Fe}_{S0}} \tag{11}$$

Similarly, the pooled hemoglobin data were simultaneously fitted using the following relationship between blood hemoglobin concentration, Hb, and Fe_{Hb}:

$$\mathrm{Hb} = \mathrm{Hb}_0\frac{\mathrm{Fe}_{Hb}}{\mathrm{Fe}_{Hb0}} \tag{12}$$

The following residual error model was applied

$$C_{obs} = C_{pred} + \varepsilon \tag{13}$$

where C_{obs} denotes the observed, C_{pred} is the model-predicted serum iron or blood hemoglobin concentration, and ε is the residual error that was assumed to be normally distributed with zero mean and standard deviation σ, defined as follows:

$$\sigma = a + bC_{pred} \tag{14}$$

where a and b are parameters estimated during the model fitting. The PK/PD model was implemented in ADAPT 5 program (16). The PK parameters were fixed. The maximum likelihood estimator was used for parameter estimation. The Student t test was applied for comparison of between the means of two groups, and ANOVA F test was used if means of more than two groups were compared.

RESULTS

Figure 2 shows the mean serum iron concentration-time courses following single administrations of Ab 12B9m along with simulated time profiles of serum hepcidin concentrations. Both IV and SC administration of a single dose of Ab 12B9m resulted in a rapid decrease in hepcidin serum concentrations from the baseline to reach a sharp nadir, followed by a rapid return to the baseline. The duration of the nadir phases was somewhat prolonged for the largest dose (50 mg/kg). The nadir values were 2.1, 0.2, and 0.02 nM for IV doses 0.5, 5, and 50 mg/kg, respectively. The analogous nadir values for the corresponding SC doses were 9.3, 7.6, and 0.18 nM. The observed serum iron responses to IV and SC doses 0.5 and 5 mg/kg were not different from the baseline except for 5 mg/kg IV where the peak reached 217 μg/dL. The serum iron concentrations corresponding to the highest IV and SC dose of 50 mg/kg increased to reach peaks of 320 and 354 μg/dL, respectively, between 24 and 48 h after dosing and, then declined to the baseline.

Hepcidin and serum iron concentrations following multiple-dose administrations of Ab 12B9m are presented in Fig. 3. Hepcidin responses to 5 and 40 mg/kg q.w. for 4 weeks exhibit oscillatory steady state where the time course after the first dose is identical to the time course after the fourth dose. Both IV and SC repeated administrations of the highest dose 300 mg/kg q.w. entirely suppressed hepcidin for 32 days and returned to the baseline levels 43 days (1032 h) after first dose. The serum iron levels spiked after each IV dose of 5 and 40 mg/kg, and then returned to the baseline. The mean of the serum iron concentration peak after the first 40 mg/kg dose, 430 ± 110 μg/dL, was slightly higher than that obtained after the third dose, 370 ± 49 μg/dL, but not significantly different ($P = 0.08$). The time courses of serum iron following multiple IV and SC doses at 300 mg/kg were also similar and did not exhibit the oscillatory pattern observed at lower doses. Instead, the serum iron response peaked after the first dose, followed by a gradual decline during subsequent doses (probably due to tolerance to drug effects), and then a rapid decrease to the baseline after treatment ended. The peak value of 418 ± 77 μg/dL after the first 300 mg/kg IV dose was similar to the peak obtained after the first 50 mg/kg IV dose ($P = 0.78$).

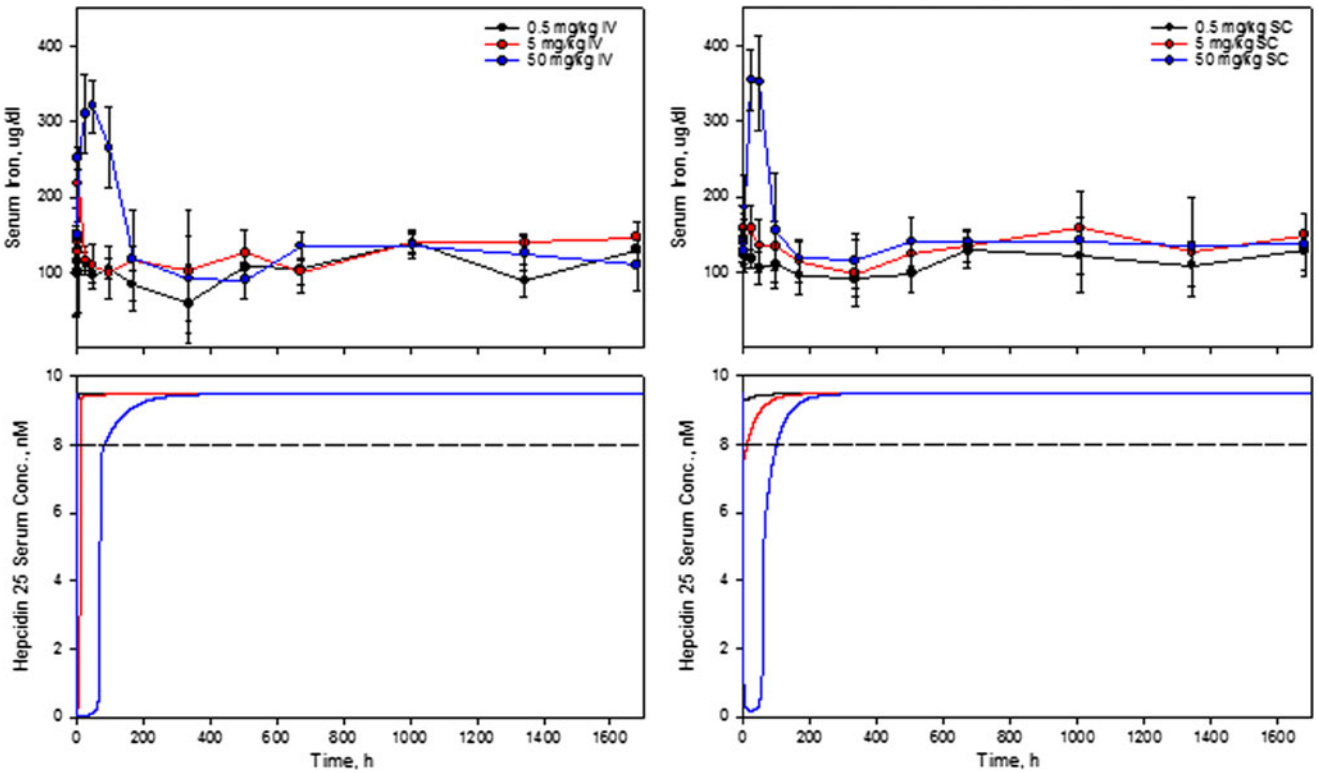

Fig. 2. Serum iron concentrations following administration a single IV and SC dose of Ab 12B9m (*top*) and corresponding hepcidin H_{25} serum concentrations (*bottom*). The iron data are presented as means (*symbols*) and standard deviations (*error bars*) of $n = 3$ animals. The hepcidin time courses were simulated according to the PK model described in Appendix (6)

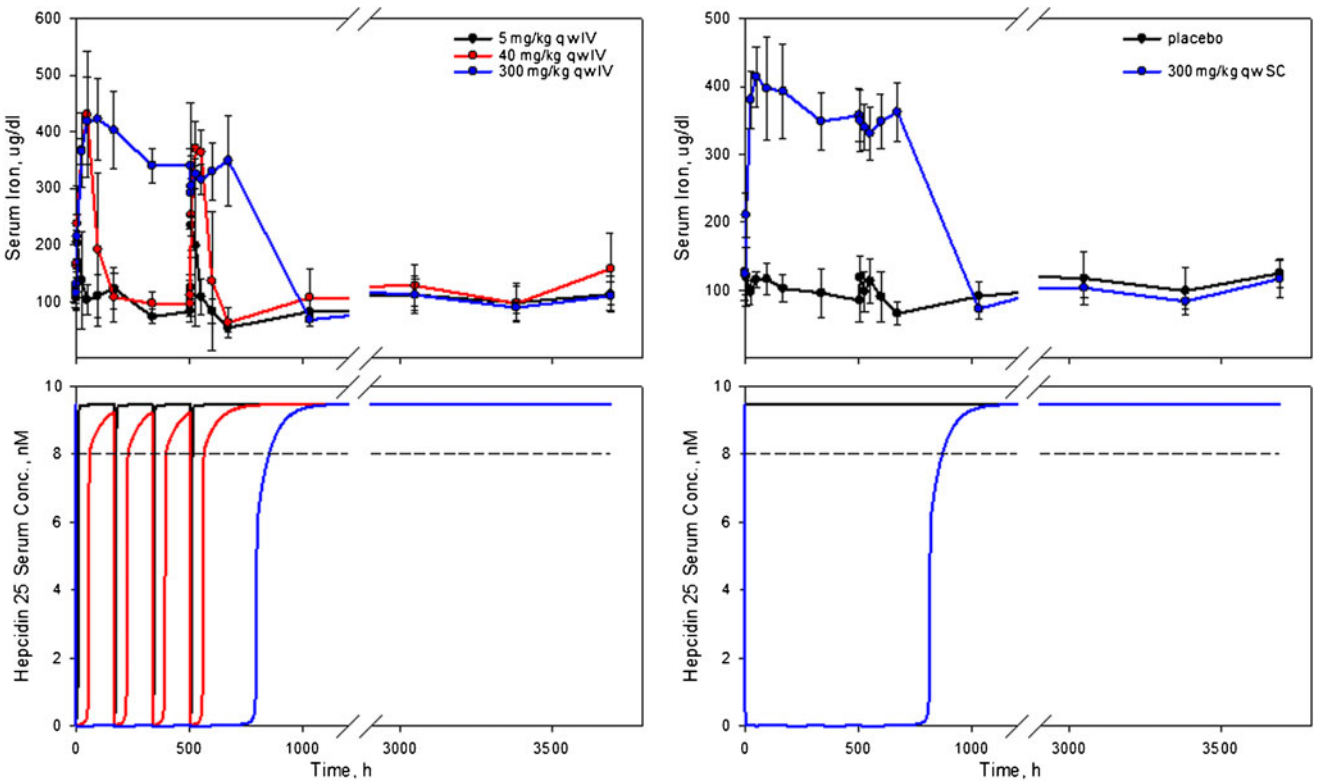

Fig. 3. Serum iron concentrations following multiple administration IV and SC doses of Ab 12B9m (*top*) and corresponding hepcidin H_{25} serum concentrations (*bottom*). The iron data are presented as means (*symbols*) and standard deviations (*error bars*) of $n = 10$ animals. The hepcidin time courses were simulated according to the PK model described in Appendix (6)

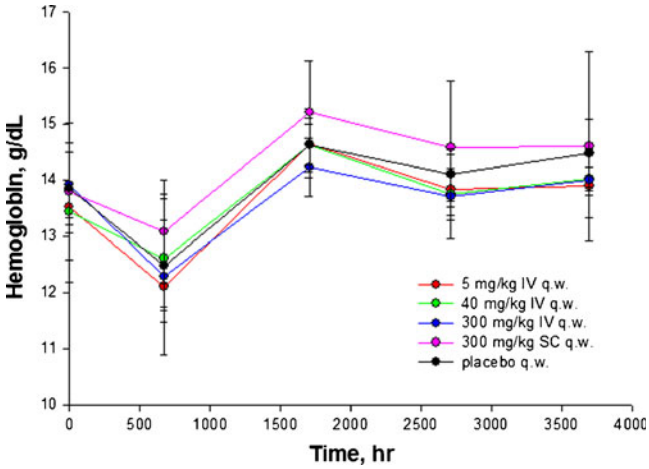

Fig. 4. Blood hemoglobin concentrations following administration of multiple IV and SC doses of Ab 12B9m. The data are presented as means (*symbols*) and standard deviations (*error bars*) of $n = 10$ animals

The mean hemoglobin levels following multiple doses of hepcidin and placebo are shown in Fig. 4. The pre-dose levels are represented at time 0 and the time courses of the treatment groups clearly mimic the Hb time course of the placebo group. Numerous blood samples were taken from animals during the treatment phase of the 1-month toxicology study, particularly after the 1st and 4th doses, which likely caused the decrease in hemoglobin levels in all animals. Blood sampling was sparse during the recovery period of the study, during which time hemoglobin rebounded. The hemoglobin measurement for the placebo group started at 13.8 ± 0.7 g/dL, decreased to the nadir of 12.9 ± 0.8 g/dL at 28 days (672 h), followed by a rebound to reach the value of 14.6 ± 0.5 g/dL around 71 days after the first dose and then

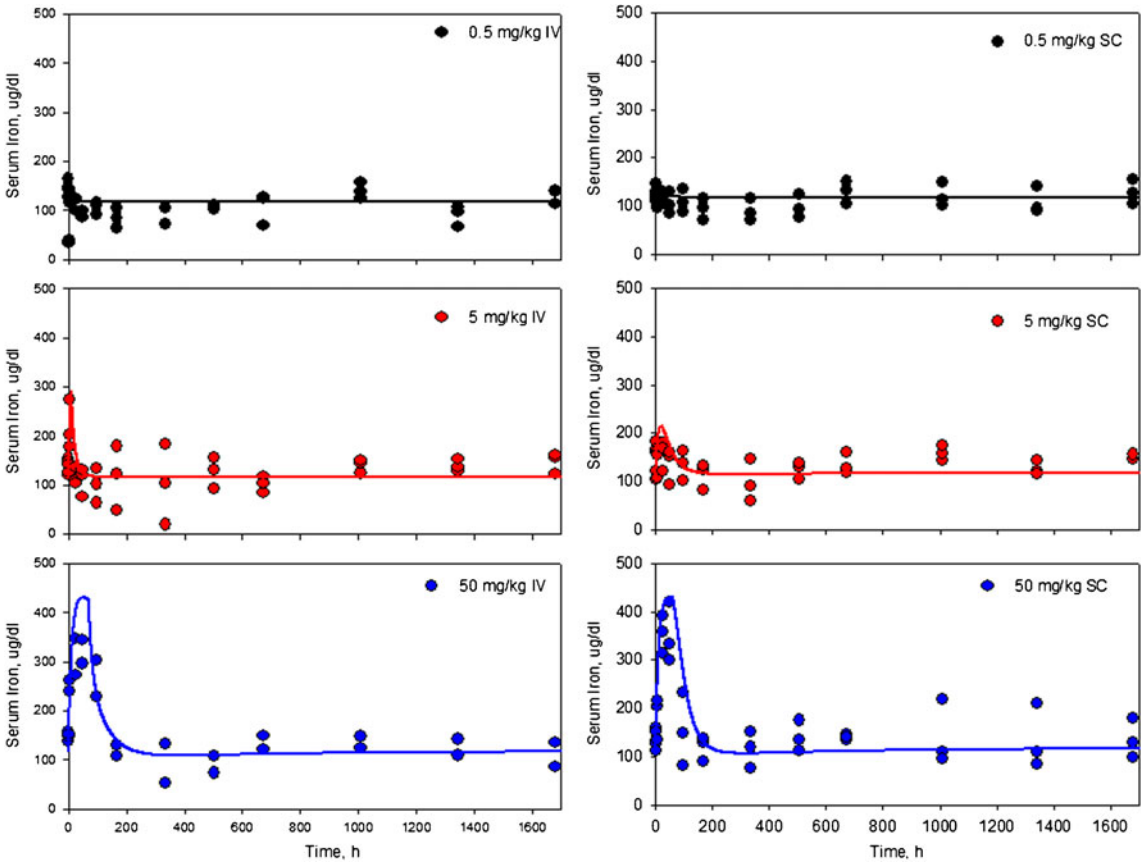

Fig. 5. The PD model fittings (*solid lines*) of the pooled individual animal iron serum concentrations (*symbols*) following administration of a single IV and SC dose of Ab 12B9m

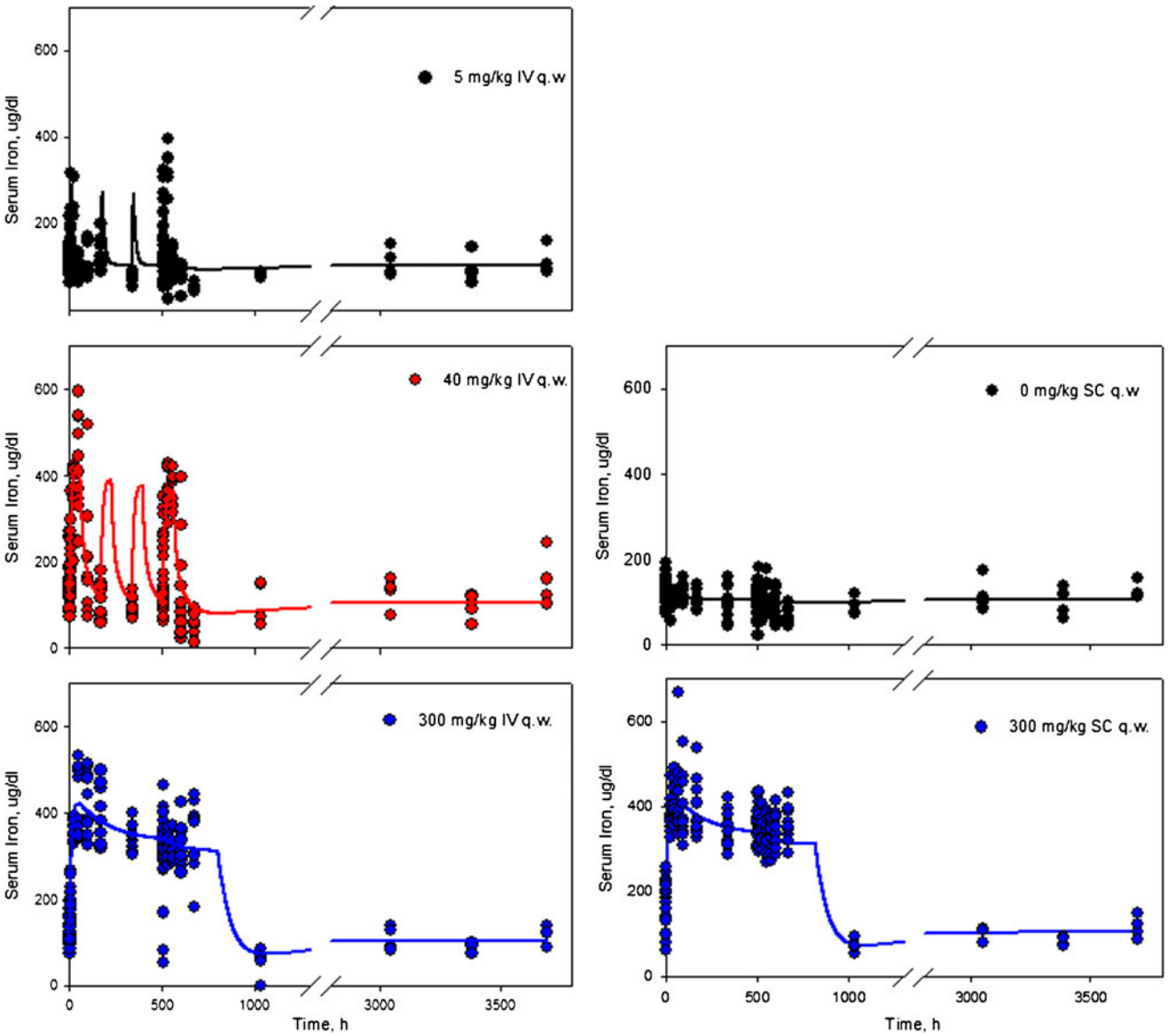

Fig. 6. The PD model fittings (*solid lines*) of the pooled individual animal iron serum concentrations (*symbols*) following administration of multiple IV and SC doses of Ab 12B9m

remained steady through subsequent measurements. Both the nadir and the rebound hemoglobin levels were significantly different from the pre-dose value ($P < 0.0001$ and $P = 0.032$, respectively). However, the hemoglobin for the placebo group was not significantly different from the treatment groups at each time point.

The pooled concentrations of serum iron from all dosing groups were fitted simultaneously and the model fittings are shown in Figs. 5 and 6. The model predictions depicted the time courses of the mean observed serum iron data shown in Figs. 2 and 3. The PD model accurately described the serum iron peaks following single-dose administrations except for 50 mg/kg SC where the peak was slightly under predicted. The peaks and troughs of serum iron concentrations for multiple doses exhibited the tolerance that was observed in the data. The C_{Fe} time profiles gradually declined following the peak after the first dose to end in a rapid return towards the baseline after the last dose. The PD model predictions for those highest doses administered repeatedly showed a small rebound (a decrease below the baseline) after the decline following the last dose. The percent decrease was 33.3% (both IV and SC).

Figure 7 shows the hemoglobin data fitted by the PD model. The model-predicted response exhibited rapid declines at 0 and 21 days (504 h) caused by the blood withdrawals followed by a gradual return to the baseline value of 13.9 g/dL reached approximately on day 45 (1080 h). The hemoglobin responses did not depend on doses and were identical for dosing groups including placebo. The model-predicted decrease in hemoglobin due to blood withdrawal was 5.3 g/dL. Given blood volume of 30 mL drawn from each animal over the 3-week period during this study, the blood loss due to frequent sampling was approximately 10% of the total blood volume, which should have resulted in a decrease of Hb about 1.4 g/dL. The model over-prediction is caused be modeling blood loss as a two events rather than multiple event process.

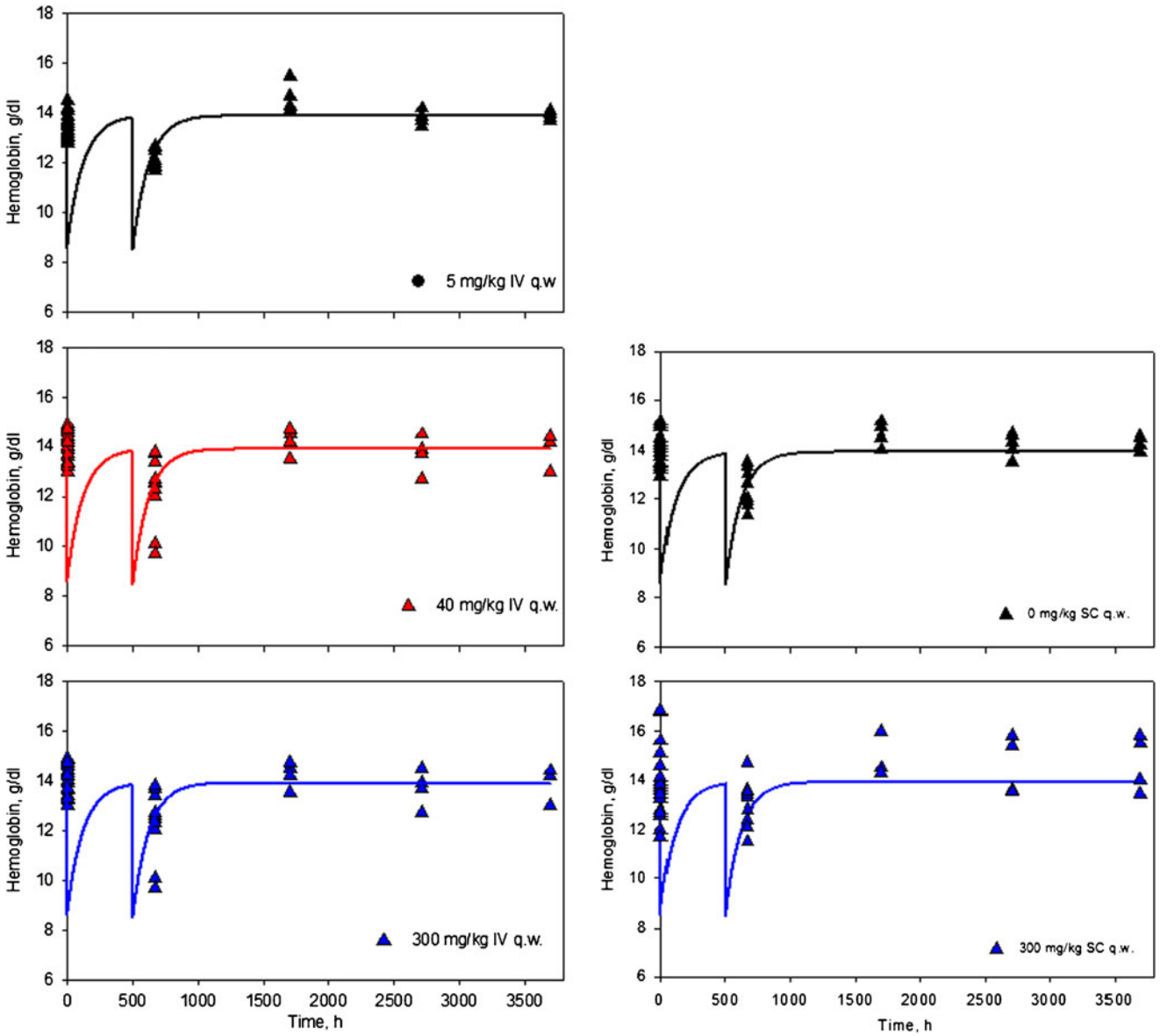

Fig. 7. The PD model fittings (*solid lines*) of the pooled individual animal hemoglobin levels (*symbols*) following administration of multiple IV and SC doses of Ab 12B9m

Table I. Parameter Estimates for the PD Model Obtained by Fitting Iron Serum and Blood Hemoglobin Concentration Data

Parameter	Estimate	CV%
k_S/Fe_{S0} (h^{-1})	0.113	26.5
k_{SL} (h^{-1})	0.0826	8.47
k_{LS} (h^{-1})	0.000848	39.8
k_M (h^{-1})	0.00191	31.4
k_{Hb} (h^{-1})	0.00817	63.6
C_{Fe0} (μg/dL)	117	1.70
Hb_0 (g/dL)	13.9	0.5
I_{max}	1[a]	
IC_{50} (nM)	0.398	3.0
γ	5.03	13.7
Fr	0.382	91.4
AIC	12,649	

CV% percent coefficient of variation, *AIC* Akaike Information Criterion
[a] Parameter was fixed

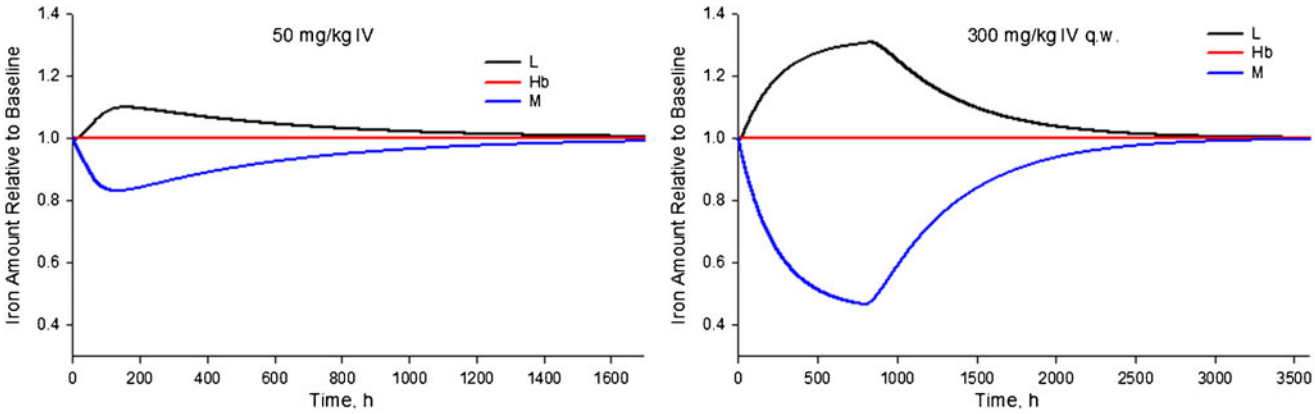

Fig. 8. Time courses of the amount of iron in L, Hb, and M pools relatively to the baseline values following a single IV dose of 50 mg/kg (*left*) and multiple IV doses of 300 mg/kg q.w.

The estimates of the PD parameters are shown in Table I. They were obtained with reasonable precisions with the percent coefficient of variation less than 40%, except for the parameters Fr and k_{Hb}, where the percent coefficient of variation (CV%) were 91.4% and 63.6%, respectively. These two parameters were also highly correlated (0.99). The model was not capable of predicting accurately the baseline iron levels in the liver and macrophage pools, however, the ratios $Fe_{L0}/Fe_{S0} = 97.4$, $Fe_{M0}/Fe_{S0} = 59.4$, and $Fe_{Hb0}/Fe_{S0} = 13.8$ were calculated from Eq. 6a, 6b, and 6c. The reciprocal of a first-

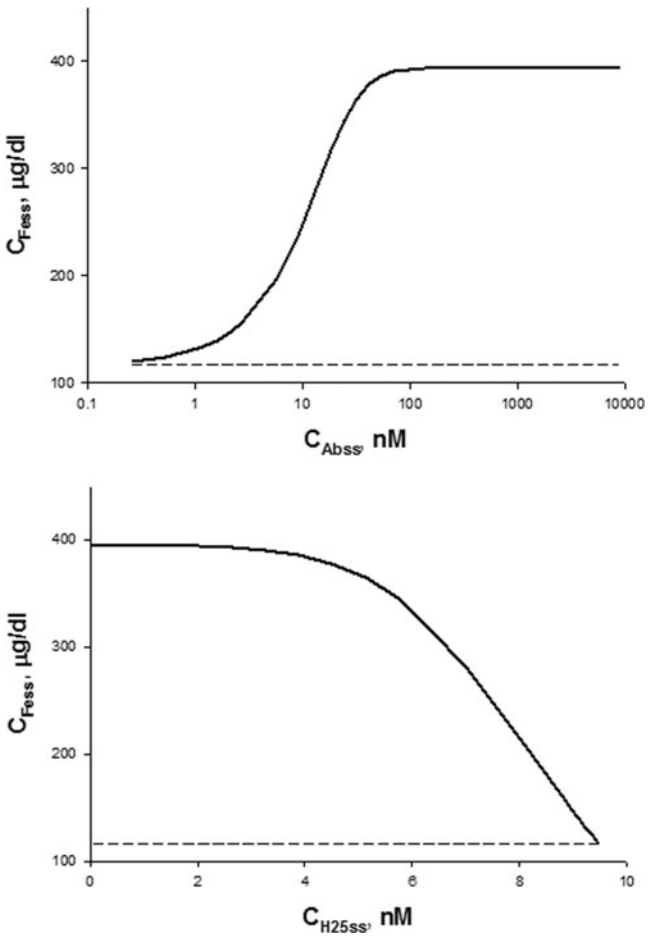

Fig. 9. Simulated plots of steady-state serum iron concentration C_{Fess} *vs*. steady-state Ab 12B9m serum concentration C_{Abss} (*top*) and C_{Fess} *vs*. steady-state hepcidin H_{25} serum concentration C_{H25ss} (*bottom*). The *dashed line* denotes baseline serum iron C_{F0}. Parameter values used for simulations are presented in Table I

Table II. Comparison of Pharmacodynamics Model First-Order Rate Constants with Their Values Reported in Literature for Humans

Parameter	Estimated value	Literature value	Calculation	Reference
k_S/Fe_{S0} (day^{-1})	2.71	12.2	k_{21}	(10)
k_{SL} (day^{-1})	1.98	3.6	k_{51}	(10)
k_{LS} (day^{-1})	0.020	0.0035	ln2/200	(18)
k_M (day^{-1})	0.0458	0.31	k_{17}	(10)
k_{Hb} (day^{-1})	0.196	0.0066	ln2/105	(9)

order rate constant can be interpreted as a mean residence time an iron molecule stays in the pool. Alternatively, one can calculate its half-life in the pool as the product of ln2 and the mean residence time. Consequently, $1/k_{LS} = 49.1$ days is an estimate of the average storage time of the iron in the liver and $1/k_M = 21.8$ days in the macrophage reticuloendothelial pool. The average time iron is bound to hemoglobin is $1/k_{Hb} = 5.1$ days which is much shorter than the mean RBC lifespan of 80 days for cynomolgus monkeys reported in the literature (17). The corresponding half-lives are $\ln2/k_{LS} = 34.0$, $\ln2/k_M = 15.1$, and $\ln2/k_{Hb} = 3.5$ days. The zero-order transfer rate of iron from the serum pool into hemoglobin was identifiable only as a ratio $k_S/Fe_{S0} = 0.113\ h^{-1}$. A very precise estimate of the baseline iron serum concentration of $C_{Fe0} = 117$ μg/dL (CV = 1.7%) was obtained from the placebo serum iron data. Similarly, the baseline hemoglobin level was estimated as $Hb_0 = 13.9$ g/dL (CV = 0.5%). The PD model contained two parameters specific to hepcidin's mechanism of action (besides I_{max}), $IC_{50} = 0.389$ nM and $\gamma = 5.03$. The estimated IC_{50} value was 23.8-fold lower than the estimated baseline of the serum hepcidin concentration $C_{H25,0} = 9.48$ nM, which implied 96.0% of the maximal inhibition of the iron transport by hepcidin at the baseline conditions. The fraction of serum iron lost due to blood drawing was 0.382.

The simulations of the relative changes in iron content for hemoglobin, reticuloendothelial macrophages, and liver pools following IV administration of a single dose of 50 mg/kg IV and multiple doses of 300 mg/kg hepcidin are shown in Fig. 8. The hemoglobin response did not change. The fastest response to the single dose was observed for the Fe_M compartment where the iron decreased to a nadir 83.1% of the baseline value around 126 h after the Ab 12B9m injection, and then returned to the baseline reaching 99.1% after 10 weeks. The iron in liver increased up to 110% at 152 h and then returned to baseline. After 10 weeks, Fe_L reached 101% of the baseline. Administration of 300 mg/kg q.w. for 4 weeks resulted in more pronounced iron responses. The nadir of the Fe_M was 46.6% and occurred at 797 h, whereas the peak for the Fe_L was 131% and occurred at 825 h. The levels of Fe_M and Fe_L responses after 10 weeks were 88.7% and 107%, respectively.

To assess a dose–response relationship between Ab 12B9m and serum iron, we performed simulations of these variables for continuous intravenous infusions of the antibody for escalating doses to a point at which steady state was reached. Figure 9 shows the relationship between the steady-state serum concentrations of Ab 12B9m and Fe_S. Additionally, we included an analogous relationship between the steady-state concentration of serum hepcidin and Fe_S. The serum iron concetration at steady-state *vs.* Ab 12B9m serum concentration at steady-state response curve increases from the baseline value $C_{Fe0} = 117$ μg/dL to reach a plateau of $C_{Femax} = 394$ μg/dL for $C_{Abss} > 100$ nM. The corresponding $EC_{Abss50} = 11$ nM is 10,000-fold higher than the equilibrium-binding dissociation constant for the antibody ($k_{DH} = 0.001$ nM). The serum iron concentration at steady-state *vs.* H_{25} serum concentration at steady-state curve reflects increased Fe_S values with decreasing steady-state hepcidin serum concentrations to reach the plateau for $C_{H25ss} < 3$ nM.

DISCUSSION

We have developed a pharmacodynamic model describing the role of hepcidin H_{25} in regulating iron homeostasis and characterized the impact of hepcidin inhibition by an anti-hepcidin monoclonal antibody Ab 12B9m, by fitting the serum iron and hemoglobin data in response to single and multiple doses of Ab 12B9m. In this context, we have obtained estimates of ferrokinetic parameters as well as parameters characterizing the hepcidin inhibitory effect on ferroportin. The naïve pooled data analysis was selected to be consistent with the analysis of PK data where this approach was applied. Given much larger inter-subject variability of PD data, a preferable technique of parameter estimation would have been population analysis. While this approach could have resulted in more accurate parameter estimates, the naïve pooled data approach was sufficient to properly address the key relevant questions which arose during the development of Ab 12B9m.

A comparison of estimates of the first-order transfer rate constants in our model with analogous values reported in literature for humans is shown in Table II. The processing of erythrocyte iron by the reticuloendothelial cells has been characterized by kinetic measurements of blood radioactivity made after the intravenous injection of heat-damaged erythrocytes labeled with ^{59}Fe and transferrin-bound ^{55}Fe in dogs (18). There was an initial processing period within the reticuloendothelial cell, after which labeled iron either rapidly returned to circulation with the half-life of 34 min or was transferred to a slowly exchanging pool of storage iron within the reticuloendothelial cells. The half-life of the iron release from the storage pool was estimated as 7 days. These half-lives can serve as means to approximate the mean residence times of the rapid exchange and storage pools in the reticuloendothelial macrophages using the formula $t_{1/2}/\ln(2)$, yielding 0.82 and 242 h. Our estimate of the mean residence time for the reticuloendothelial macrophage pool calculated as $1/k_M$ is 524 h. This exceeds by more than twofold the estimates of residence times in the reticuloendothelial macrophage storage pool cited above as well as in other reports

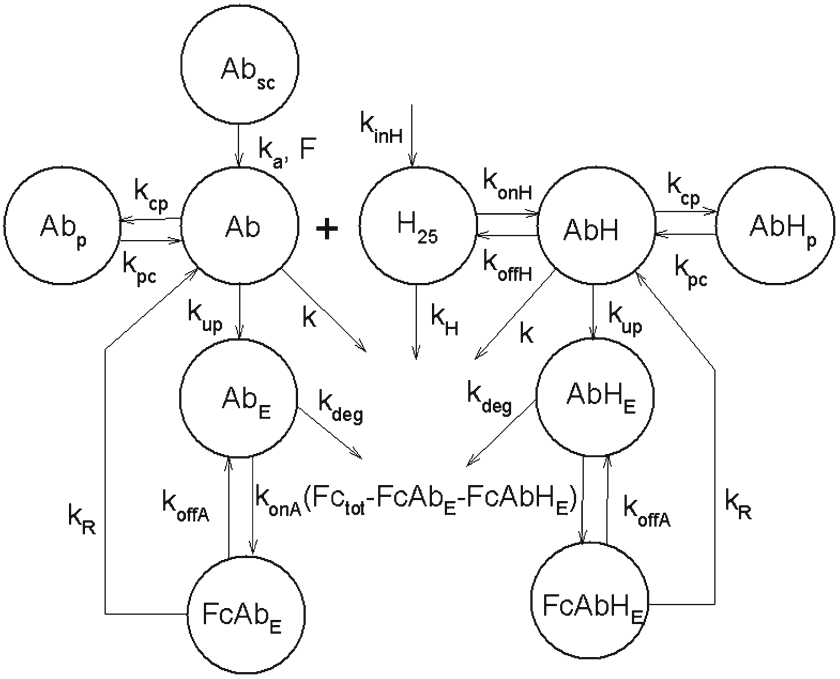

Fig. 10. Schematic of pharmacokinetic model for H_{25} and Ab 12B9m in cynomolgus monkeys

on ferrokinetics in man (10,14). The reported first-order elimination rate constant from the parenchymal tissues in normal subject was 0.35 h^{-1}, which translates to 68.1 h of mean residence time (10). The same constant estimated for mouse liver was 0.0058 h^{-1}, yielding 171 h of mean residence time (11). Our estimate of the mean residence time of iron in the parenchymal liver cell is $1/k_{LS} = 1180.0$ h. Both estimates of the residence times in the liver and macrophage storage pools are much shorter than the lifespan ranges for those cells. The mean lifespan of mammalian hepatocytes is between 200 and 300 days (18). The average lifespan of human macrophages is several months (19). The ferroportin-mediated transport of iron from the deep storage compartments to the blood plasma in response to hepcidin inhibition exhibits a slower kinetics than a transport of exogenously administered radiolabeled iron typically used in the ferrokinetic studies. This could be a possible explanation of the discrepancies between our estimates and the reported values for the iron average residence times in the storage pools based on the tracer kinetics of ^{59}Fe. The value of the constant $k_{SL} = 0.0826$ h^{-1} is close to the range 0.12–0.19 h^{-1} reported in (10) for the first-order rate constant k_{51} of the transport of serum iron to the nonerythroid parenchymal storage pool.

We selected k_S as a zero-order rate of iron transfer from serum to hemoglobin pools, under the assumption of the proportionality between iron amount and hemoglobin levels, after trying a model where it was a first-order rate constant and another model with the Michaelis-Menten elimination. In the latter, the constant k_S could be interpreted as V_{max}, a rate that is the maximum of the nonlinear process saturated by the much higher values than K_m baseline serum iron concentration C_{Fe0}. Our attempt to estimate the Michaelis-Menten parameters V_{max} and K_m was unsuccessful. The model with k_S as a first-order rate constant grossly over-predicted hemoglobin concentrations as shown in the Supplementary Material. Since the hemoglobin response for the placebo group was not significantly different from the treatment groups, the only perturbation of the hemoglobin was due to blood sampling. Consequently, the hemoglobin data were not informative about the hepcidin inhibitory effect, rendering the transfer rate k_S as a zero-order constant. Due to limited data, only the ratio k_S/Fe_{S0} was estimated. The zero-order process k_S made the hemoglobin levels insensitive to changes in serum iron levels. This resulted in under-prediction of the observed rebound in hemoglobin response. The hemoglobin rebound is most likely a result of stimulated by bleeding erythropoiesis. The first-order elimination from the hemoglobin pool was reported as 0.00167 h^{-1} for mouse with the mean transit time of 25 days (11). This time is consistent with the mean mouse RBC lifespan (20). Our estimate of k_{Hb} yielded an iron mean residence time in the hemoglobin pool of 5.1 days which is by far less than the average RBC lifespan of 90 days in cynomolgus monkeys (17). The estimate of k_{Hb} was based on the hemoglobin data and it was determined by the time the hemoglobin returned to the baseline after the blood draws. Such data provided limited information about k_{Hb} as seen by a high CV of its estimate. The precision of parameter estimates might be improved if additional data with stimulated hemoglobin response were available. Intravenous iron supplementation has been reported to increase Hb blood concentrations (21). Since in this target population iron levels are sufficiently high to avoid any restriction of the erythropoiesis, it is expected that further increases in serum iron does not result in any significant change in hemoglobin as this is clearly seen in Fig. 8. However, we do not know if that would be true in anemic animals, where the iron levels might be restricting the erythropoiesis and, consequently, serum iron increases as a consequence of the drug administration may lead to an increase in hemoglobin.

Table III. Parameter Estimates for the PK Model of Anti-hepcidin Monoclonal Antibody Ab 12B9m Obtained from (6)

Parameter	Estimate	CV%
k_a (h^{-1})	0.0278	6.0
F	0.860	2.6
CL (L kg^{-1} h^{-1})	0[a]	N/A
V_c (L/kg)	0.0438	3.8
V_p (L/kg)	0.00483	51.6
Q (L kg^{-1} h^{-1})	0.00245	141
$H_{25,0}$ (nmol/kg)	0.415	6.2
k_{up} (h^{-1})	0.0150	10.8
k_{onH} (nM^{-1} h^{-1})	0.543	53.0
k_{DH} (nM)	0.001[a]	N/A
Fc_{tot} (nmol/kg)	1503	14.9
k_H (h^{-1})	18.3	6.8
$k_{DA} \cdot V_E$ (nmol/kg)	312	26.3
k_{deg} (h^{-1})	0.0208	32.3

[a] Parameter was fixed

The estimate of IC_{50} allowed us to calculate the efficiency of the inhibition of the ferroportin-mediated transport of the iron from the storage pools to plasma. At the baseline conditions, this is 96.0%, indicating that only a small fraction of stored iron is released to the circulation. The maximum inhibition parameter I_{max} was not estimable and eventually fixed at 1. The Hill sigmoidal shape factor $\gamma = 5.03$ implies a steep relationship between the inhibitory effect of hepcidin and its serum concentration. Our study demonstrated that only the highest weekly dose of 300 mg/kg was able to maintain the hepcidin levels below IC_{50} and consequently maintain elevated serum iron. This implies that a hepcidin concentration resulting in 50% of the ferroportin activity, IC_{50}, can serve as a therapeutic target not only for Ab 12B9m but also for other hepcidin inhibitors.

The iron kinetics model developed accounts for the four largest iron pools: hemoglobin in bone marrow and circulating RBCs, liver parenchyma, macrophages of the reticuloendothelial system, and iron trapped in plasma transferrin. The iron distribution to myoglobin in skeletal and cardiac muscle and other tissues was not included in the model. Since the anti-hepcidin Ab 12B9m treatment perturbed the serum iron data for no more than 600 h, the contribution to the serum iron pool from the input dietary iron and loss from sloughed mucosal cells, desquamation, and menstruation were not considered substantial and ignored by the model. Consequently, there was no input or output in the model, resulting in a closed system. The available data could not support a more complex model without parameter identifiability problems. Due to these reasons, the hemoglobin iron pool should be considered as a hybrid bone marrow early and late erythropoietic pools, and circulating RBCs included in reported in the literature ferrokinetic models (8,11,13,22). Also, the iron pool Fe_M represents the lumped transit and storage pools of the reticuloendothelial system (10), and the liver pool Fe_L encompasses tissue exchangeable and tissue storage pools (22).

The serum iron data obtained after multiple doses of Ab 12B9m exhibits tolerance and rebound phenomena (a decrease below the baseline values) that can be attributed to the depletion of the liver and reticuloendothelial macrophage storage compartments. This is consistent with a time course of an indirect pharmacological response caused by the drug acting on a precursor of the effect compartment (23). Similar tolerance and rebound phenomena have been reported for a reticulocyte response to the treatment with erythropoiesis-stimulating agents (24–28). The mechanisms underlying such response remain unclear. Iron is essential for development of erythroblasts into erythrocytes. During stressed erythropoiesis, the demand for iron increases leading to the depletion of the iron storage pools (29,30). Erythropoietin administration has been reported to cause a reduction in circulating hepcidin (31). This resembles the iron kinetics presented here due to hepcidin inhibition by Ab 12B9m. Consequently, one might hypothesize that the tolerance and rebound in the reticulocyte response during stressed erythropoiesis are caused by the tolerance and rebound in serum iron due to the depletion of iron storage pools.

Our simulations show that inhibition of hepcidin results in an increase of serum iron as well as accumulation of iron in the liver. Since the hemoglobin iron remained relatively constant, these increases were at the expense of depletion of the iron from reticuloendothelial macrophages. Because iron circulation was assumed to be a closed system, a decrease in the macrophage iron matched the sum of increases of iron in serum and liver. Both the duration and extent of iron change in these pools increased with increasing doses of Ab 12B9m.

Increased hepcidin levels and reduced ferroportin activity are considered major factors in anemia of chronic disease (ACD) (4). The inflammatory cytokine response stimulates hepcidin production leading to iron sequestration in macrophages, which results in low levels of circulating iron and eventually anemia (32). Current therapeutic management of ACD can involve increasing hemoglobin levels by blood transfusions and administration of erythropoiesis-stimulating agents and iron. However, such a treatment can have limited effectiveness in some patients and can lead to adverse events. Moreover, it does not reduce the elevated hepcidin levels. Hepcidin inhibitors such as Ab 12B9m can effectively decrease hepcidin plasma concentration for a prolonged time. Our study demonstrated that a hepcidin concentration resulting in 50% of the ferroportin activity (IC_{50}) can serve as a therapeutic target for other hepcidin inhibitors. Since the hepcidin concentration in ACD patients is elevated, one can expect larger doses than for healthy subjects to maintain the hepcidin concentration below the IC_{50} and observe the same effect.

Previously, we have established that free Ab 12B9m exhibits nonlinear kinetics with a terminal half-life of 16.5 days and free H_{25} has a high turnover rate with a production rate of 7.6 nmol kg^{-1} h^{-1} and elimination half-life of 2.3 min (6). Consequently, weekly doses higher than 150 mg/kg, administered by SC or IV route, are needed to maintain free H_{25} below 0.1 nM, approximately 99% suppression. These findings confirm that the main determinants guiding the dose selection for monoclonal antibody are both the target turnover and the drug pharmacokinetics.

In summary, the ferrokinetic model accounting for hepcidin control of the iron homeostasis in monkeys adequately described the serum iron and hemoglobin time courses following single and multiple doses of anti-hepcidin monoclonal antibody Ab 12B9m. The model simplified existing ferrokinetic models to four iron compartments encompassing serum, liver, erythrocyte hemoglobin, and reticuloendothelial macrophages. The data supported the postulated mechanism of hepcidin inhibition of the ferroportin-mediated transport of the iron from the liver and reticuloendothelial macrophage storage pools. The Ab 12B9m-induced inhibition of hepcidin resulted in a temporal increase in serum and hemoglobin iron and a decrease in the stored iron amounts with no effect on hemoglobin levels. The data permitted estimation of only the iron kinetic parameters, the baseline serum iron concentration and hemoglobin, along with two parameters characterizing the inhibitory effect of hepcidin. The hepcidin concentration resulting in 50% of the ferroportin activity IC_{50} can be considered as a therapeutic target. The model predicted the depletion of the iron storage compartments that resulted in the tolerance and rebound in the observed serum iron levels. An adequate description of the iron kinetics due to the hepcidin inhibition is of importance in understanding the mechanisms of iron-restricted erythropoiesis caused by therapy with erythropoiesis-stimulating agents (33).

APPENDIX

PK model of anti-hepcidin monoclonal antibody Ab 12B9m.

The PK model description for Ab 12B9m has been excerpted from the original publication Xiao *et al.* (6). A schematic of the PK model is shown in Fig. 10. Ab_{sc} represents the SC depot for Ab 12B9m SC dosing. Ab 12B9m and Ab 12B9m-H_{25} complex distribute into their central compartments (Ab and AbH), peripheral compartments (Ab_p and AbH_p), and endosome compartments (Ab_E and AbH_E). In endosome, Ab 12B9m and Ab 12B9m-H_{25} complex binds to FcRn to form complexes ($FcAb_E$ and $FcAbH_E$). The intercompartment distribution was described with a set of first-order rate constants (k_{cp}, k_{pc}, k_{up}, and k_R), and elimination from Ab and AbH follows first-order kinetics (k). It was assumed that Ab 12B9m and Ab 12B9m-H_{25} complex share the same parameter as listed above. H_{25} is produced at a constant rate (k_{inH}) and eliminated with first-order kinetics (k_H). In serum, the binding between Ab 12B9m and H_{25} is governed by the association rate constant (k_{onH}) and the dissociation rate constant (k_{offH}); similarly, in endosome the binding of Ab 12B9m and Ab 12B9m-H_{25} complex to FcRn is described by k_{onA} and k_{offA}.

$$\frac{d\mathrm{Ab_{SC}}}{dt} = -F\cdot k_a\cdot A_{SC} \tag{11}$$

$$\frac{d\mathrm{Ab}}{dt} = F\cdot k_a\cdot A_{SC} - \left(k + k_{up} + k_{cp}\right)\cdot \mathrm{Ab} - k_{onH}\cdot \mathrm{H_{25}}\cdot \mathrm{Ab}/V_c + k_{offH}\cdot \mathrm{AbH} + k_R\cdot \mathrm{FcAb_E} + k_{pc}\cdot \mathrm{Ab_p} \tag{12}$$

$$\frac{d\mathrm{Ab_p}}{dt} = k_{cp}\cdot \mathrm{Ab} - k_{pc}\cdot \mathrm{Ab_p} \tag{13}$$

$$\frac{d\mathrm{H_{25}}}{dt} = k_{inH} - k_H\cdot H_{25} - k_{onH}\cdot \mathrm{H_{25}}\cdot A_b/V_c + k_{offH}\cdot \mathrm{AbH} \tag{14}$$

$$\frac{d\mathrm{AbH}}{dt} = k_{onH}\cdot \mathrm{H_{25}}\cdot \mathrm{Ab}/V_c - \left(k_{offH} + k + k_{up} + k_{cp}\right)\cdot \mathrm{AbH} + k_{pc}\cdot \mathrm{AbH_p} + k_R\cdot \mathrm{FcAbH_E} \tag{15}$$

$$\frac{d\mathrm{AbH_p}}{dt} = k_{cp}\cdot \mathrm{AbH} - k_{pc}\cdot \mathrm{AbH_p} \tag{16}$$

$$\frac{d\mathrm{Ab_{Etot}}}{dt} = k_{up}\cdot \mathrm{Ab} - k_{deg}\cdot \mathrm{Ab_E} - k_R\cdot \mathrm{FcAb_E} \tag{17}$$

$$\frac{d\mathrm{AbH_{Etot}}}{dt} = k_{up}\cdot \mathrm{AbH} - k_{deg}\cdot \mathrm{AbH_E} - k_R\cdot \mathrm{FcAbH_E} \tag{18}$$

where V_c denotes the central compartment volume of Ab 12B9m, which was assumed to be the same for hepcidin H_{25} and the Ab 12B9m-H_{25} complex; Ab_{Etot} and AbH_{Etot} are the total amounts, respectively, of Ab 12B9m and Ab 12B9m-H_{25} in the endosomal compartments:

$$\mathrm{Ab_{Etot}} = \mathrm{Ab_E} + \mathrm{FcAb_E} \tag{19a}$$

and

$$\mathrm{AbH_{Etot}} = \mathrm{AbH_E} + \mathrm{FcAbH_E} \tag{19b}$$

The free and bound endosomal antibodies were calculated according to the equilibrium assumption:

$$\mathrm{Ab_E} = \frac{\mathrm{Ab_{Etot}} \cdot (K_{\mathrm{DA}} \cdot V_{\mathrm{E}} + \mathrm{Ab_E} + \mathrm{AbH_E})}{K_{\mathrm{DA}} \cdot V_{\mathrm{E}} + \mathrm{Fc_{tot}} + \mathrm{Ab}_E + \mathrm{AbH_E}} \tag{20}$$

and

$$\mathrm{AbH_E} = \frac{\mathrm{AbH_{Etot}} \cdot (K_{\mathrm{DA}} \cdot V_{\mathrm{E}} + \mathrm{Ab_E} + \mathrm{AbH_E})}{K_{\mathrm{DA}} \cdot V_{\mathrm{E}} + \mathrm{Fc_{tot}} + \mathrm{Ab_E} + \mathrm{AbH_E}} \tag{21}$$

where

$$\mathrm{Ab_E} + \mathrm{AbH_E} = \frac{1}{2}(\mathrm{Ab_{Etot}} + \mathrm{AbH_{Etot}} - K_{\mathrm{DA}} \cdot V_{\mathrm{E}} - \mathrm{Fc_{tot}}) + \frac{1}{2}\sqrt{(\mathrm{Ab_{Etot}} + \mathrm{AbH_{Etot}} - K_{\mathrm{DA}} \cdot V_{\mathrm{E}} - \mathrm{Fc_{tot}})^2 + 4 \cdot (\mathrm{Ab_{Etot}} + \mathrm{AbH_{Etot}}) \cdot K_{\mathrm{DA}} \cdot V_{\mathrm{E}}} \tag{22}$$

$$\mathrm{FcAb_E} = \frac{\mathrm{Fc_{tot}} \cdot \mathrm{Ab_E}}{K_{\mathrm{DA}} \cdot V_{\mathrm{E}} + \mathrm{Ab_E} + \mathrm{AbH_E}} \tag{23}$$

$$\mathrm{FcAbH_E} = \frac{\mathrm{Fc_{tot}} \cdot \mathrm{AbH_E}}{K_{\mathrm{DA}} \cdot V_{\mathrm{E}} + \mathrm{Ab_E} + \mathrm{AbH_E}} \tag{24}$$

The initial conditions for the model variables were zero except for $\mathrm{Ab_{SC}}$, Ab, and $\mathrm{H_{25}}$. The initial values of $\mathrm{Ab_{SC}}$ and Ab were the first doses administered SC or IV, whereas the initial value for $\mathrm{H_{25}}$ was the baseline $\mathrm{H_{25}}$ serum amount $\mathrm{H_{25,0}}$. The steady state for Eq. 12 resulted in the following baseline equation:

$$k_{\mathrm{inH}} = k_{\mathrm{H}} \cdot H_{25,0} \tag{25}$$

The linear disposition parameters for Ab 12B9m were re-parameterized in terms of clearances and volumes:

$$k = \frac{\mathrm{CL}}{V_{\mathrm{c}}} \tag{26}$$

and

$$k_{\mathrm{cp}} = \frac{Q}{V_{\mathrm{c}}} \tag{27a}$$

and

$$k_{\mathrm{pc}} = \frac{Q}{V_{\mathrm{p}}} \tag{27b}$$

where Q denotes the distributional clearance and V_{p} is the volume of the peripheral compartment. Total Ab 12B9m and total $\mathrm{H_{25}}$ serum concentrations were expressed as

$$C_{\mathrm{Abtot}} = \frac{\mathrm{Ab} + \mathrm{AbH}}{V_{\mathrm{c}}} \tag{28a}$$

and

$$C_{\mathrm{Htot}} = \frac{\mathrm{H_{25}} + \mathrm{AbH}}{V_{\mathrm{c}}} \tag{28b}$$

The serum free hepcidin concentrations were calculated as

$$C_{\mathrm{H25}} = \frac{\mathrm{H_{25}}}{V_{\mathrm{c}}} \tag{29}$$

The values of the PK parameters are presented in Table III.

REFERENCES

1. Andrews NC. Disorders of iron metabolism. N Eng J Med. 1999;341:1986–95.
2. Ganz T. Molecular control of iron transport. J Am Soc Nephrol. 2007;18:394–400.
3. Kemna E, Pickkers P, Nemeth E, van der Hoeven H, Swinkels D. Time-course analysis of hepcidin, serum iron, and plasma cytokine levels in humans injected with LPS. Blood. 2005;106:1864–6.
4. Sun CC, Vaja V, Babitt JL, Lin HY. Targeting the hepcidin–ferroportin axis to develop new treatment strategies for anemia of chronic disease and anemia of inflammation. Am J Hematol. 2012;87:392–400.
5. Cooke KS, Hinkle B, Salimi-Moosavi H, Foltz I, King C, Rathanaswami P, *et al.* A fully human anti-hepcidin antibody modulates iron metabolism in both mice and nonhuman primates. Blood. 2013;122:3054–61.
6. Xiao JJ, Krzyzanski W, Wang Y-M, Li H, Rose MJ, Ma M, *et al.* Pharmacokinetics of anti-hepcidin monoclonal antibody Ab 12B9m and hepcidin in cynomolgus monkeys. AAPS J. 2010;12:646–57.
7. McCance RA, Widdowson EM. Absorption and excretion of iron. Lancet. 1937;230:680–4.
8. Nooney GC. An erythron-dependent model of iron kinetics. Biophys J. 1966;6:601–9.
9. Ricketts C, Jacobs A, Cavill I. Ferrokinetics and erythropoiesis in man: the measurement of effective erythropoiesis, ineffective erythropoiesis and red cell lifespan using 59Fe. Br J Haematol. 1975;31:65–75.
10. Stefanelli M, Bentley DP, Cavill I, Roeser HP. Quantitation of reticuloendothelial iron kinetics in humans. Am J Physiol Regul Integr Comp Physiol. 1984;247:842–9.
11. Lopes TJS, Luganskaja T, Spasic MV, Hentze MW, Mutzkenthaler MU, Schumann K, *et al.* System analysis of iron metabolism: the network of iron pools and fluxes. BMC Syst Biol. 2010;4:112.
12. Hosain F, Marsaglia G, Finch CA. Blood ferrokinetics in normal man. J Clin Invest. 1967;46:1–9.
13. Cook JD, Marsaglia G, Eschbach JW, Funk DD, Finch CA. Ferrokinetics: a biologic model for plasma iron exchange in man. J Clin Invest. 1970;49:197–205.
14. Fillet G, Beguin Y, Baldelli L. Model of reticuloendothelial iron metabolismin humans: abnormal behavior in idiopathic hemochromatosis and inflammation. Blood. 1989;74:844–51.
15. National Research Council of the National Academies. Guide for the care and use of laboratory animals. 8th ed. Washington DC: The National Academies Press; 2011.

16. D'Argenio DZ, Schumitzky A, Wang X. ADAPT 5 user's guide: pharmacokinetic/pharmacodynamic systems analysis software. Los Angeles: Biomedical Simulations Resource; 2009.
17. Landaw SA. Factors that accelerate or retard red blood cell senescence. Blood Cells. 1988;14:47–59.
18. Bucher NLR, Malt RA. Regeneration of liver and kidney. Boston: Little Brown; 1971.
19. Gonzalez-Mejia ME, Doseff AI. Regulation of monocytes and macrophages cell fate. Front Biosci. 2009;14:2413–31.
20. Burwell EL, Brickley BA, Finch CA. Erythrocyte life span in small animals; comparison of two methods employing radioiron. Am J Physiol. 1953;172:718–24.
21. Gaweda AE, Ginzburg YZ, Chait Y, Germain MJ, Aronoff GR, Rachmilewitz E. Iron dosing in kidney disease: inconsistency of evidence and clinical practice. Nephrol Dial Transplant. 2015;30:187–96.
22. Nathanson MH, McLaren GD. Computer simulation of iron absorption: regulation of mucosal and systemic iron kinetics in dogs. J Nutr. 1987;117:1067–75.
23. Sharma A, Ebling W, Jusko WJ. Precursor-dependent indirect pharmacodynamic response model for tolerance and rebound phenomena. J Pharm Sci. 1998;87:1577–84.
24. Ramakrishnan R, Cheung WK, Farrell F, Kelley M, Jolliffe L, Jusko WJ. Pharmacokinetic and phramacodynamic modeling of recombinant human erythropoietin after intravenous and subcutaneous single dose administrations in cynomolgus monkeys. J Pharmacol Exp Ther. 2003;306:324–31.
25. Krzyzanski W, Jusko WJ, Wacholtz MC, Minton N, Cheung WK. Pharmacokinetic and pharmacodynamic modeling of recombinant human erythropoietin after multiple subcutaneous doses in healthy subjects. Eur J Pharm Sci. 2005;26:295–306.
26. Woo S, Krzyzanski W, Jusko WJ. Pharmacokinetic and pharmacodynamic modeling of recombinant human erythropoietin after intravenous and subcutaneous administration in rats. J Pharmacol Exp Ther. 2006;319:1297–306.
27. Pérez-Ruixo JJ, Krzyzanski W, Hing J. Pharmacodynamic analysis of recombinant human erythropoietin effect on reticulocyte production rate and age distribution in healthy subjects. Clin Pharmacokinet. 2008;47:399–415.
28. Pérez-Ruixo JJ, Krzyzanski W, Bouman-Thio E, Miller B, Jang H, Bai SA, *et al*. Pharmacokinetics and pharmacodynamics of the erythropoietin mimetibody construct CNTO 528 in healthy subjects. Clin Pharmacokinet. 2009;48:601–13.
29. Andrews NC. Iron deficiency and related disorders. In: Greer JP, Foerster J, Luken JN, Roders GM, Paraskevanos F, Glader B, editors. Wintrobe's clinical hematology, vol. I. 11th ed. Philadelphia: Lippincott Williams & Wilkins; 2004.
30. Doshi S, Krzyzanski W, Yue S, Elliott S, Chow A, Pérez-Ruixo JJ. Clinical pharmacokinetics and pharmacodynamics of erythropoiesis-stimulating agents. Clin Pharmacokinet. 2013;52:1063–83.
31. Ashby DR, Gale DP, Busbridge M, Murphy KG, Duncan ND, Cairns TD, *et al*. Erythropoietin administration in humans causes a marked and prolonged reduction in circulating hepcidin. Haematologica. 2010;95:505–8.
32. Weiss G, Goodnough LT. Anemia of chronic disease. N Engl J Med. 2005;352:1011–23.
33. Goodnough LT, Nemeth E, Ganz T. Detection, evaluation, and management of iron-restricted erythropoiesis. Blood. 2010;116:4754–61.